ACS APPLIED MATERIALS & INTERFACES

Research Article

www.acsami.org

Visible-Light-Assisted Photoelectrochemical Water Oxidation by Thin Films of a Phosphonate-Functionalized Perylene Diimide Plus CoO_x Cocatalyst

Joel T. Kirner,[†] Jordan J. Stracke,[†] Brian A. Gregg,*[,‡] and Richard G. Finke*[,†]

[†]Department of Chemistry, Colorado State University, Fort Collins, Colorado 80523, United States

[‡]National Renewable Energy Laboratory, Golden, Colorado 80401, United States

Supporting Information

ABSTRACT: A novel perylene diimide dye functionalized with phosphonate groups, N,N′-bis(phosphonomethyl)-3,4,9,10-perylenediimide (PMPDI), is synthesized and characterized. Thin films of PMPDI spin-coated onto indium tin oxide (ITO) substrates are further characterized, augmented by photoelectrochemically depositing a CoO_x catalyst, and then investigated as photoanodes for water oxidation. These ITO/PMPDI/CoO_x electrodes show visible-light-assisted water oxidation with photocurrents in excess of 150 $\mu A/cm^2$ at 1.0 V applied bias vs. Ag/AgCl. Water oxidation is confirmed by the direct detection of O_2, with a faradaic efficiency of 80 ± 15% measured under 900 mV applied bias vs. Ag/AgCl. Analogous photoanodes prepared with another PDI derivative with alkyl groups in place of PMPDI's phosphonate groups do not function, providing evidence that PMPDI's phosphonate groups may be important for efficient coupling between the inorganic CoO_x catalyst and the organic dye. Our ITO/PMPDI/CoO_x anodes achieve internal quantum efficiencies for water oxidation ∼1%, and for hydroquinone oxidation of up to ∼6%. The novelty of our system is that, to the best of our knowledge, it is the first device to achieve photoelectrochemically driven water oxidation by a single-layer molecular organic semiconductor thin film coupled to a water-oxidation catalyst.

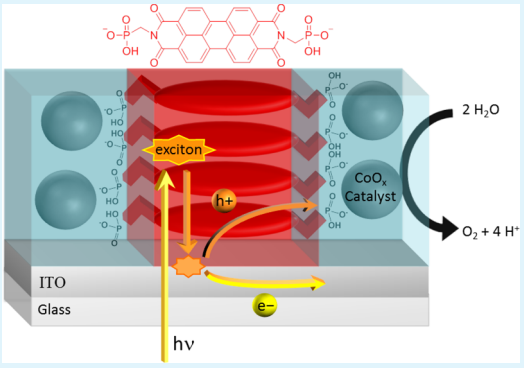

KEYWORDS: *photoelectrochemical, catalysis, water oxidation, perylene diimide, cobalt oxide, molecular semiconductor, organic thin film*

INTRODUCTION

The growing need for clean and renewable energy has led to considerable interest in the development of systems to harvest and store earth's abundant solar energy resources.[1] One promising solution is to store solar energy in the form of chemical bonds by forming solar fuels such as hydrogen gas. Indeed, the efficient photocatalytic conversion of liquid water to hydrogen and oxygen gases by artificial photosynthesis has been named as one of the "Holy Grails of Chemistry".[2,3] Since Honda and Fujishima first reported light-induced water oxidation by a TiO_2 semiconductor electrode,[4] photoelectrochemical water-splitting systems have received a great deal of attention. Although several inorganic solar water-splitting systems have achieved solar-to-hydrogen efficiencies above 10%[5−7] (the threshold for practical commercialization),[3] they are limited by the use of expensive materials or by poor long-term stability. It is, therefore, of continuing, significant interest to study alternative water-splitting systems based on semiconductors and catalysts that are composed of cheap and abundant materials.

Organic semiconductors are promising materials for electronics and photovoltaics due to the synthetic tunabilty of their properties, to their low cost, and to the low-temperature manufacturing processes they generally have available. If a suitable system were found, then these three favorable properties could help make organic-semiconductor-based water-splitting systems economically viable. Several examples of water-splitting photoelectrochemical cells employing organic materials are present in the literature.[8−17] These systems generally use organic or organometallic dyes as light collectors (a one electron/hole per photon process), coupled with catalysts to assist in water oxidation (a multi-electron process). Architectures include organic photovoltaic bilayers,[8,9] trilayers,[10] and dye-sensitized mesoporous semiconductor architectures using either organometallic[11−16] or organic polymer dye sensitizers.[17]

The hypothesis on which the current research is based is that perylene diimide dyes (PDI dyes; see the list of abbreviations at the end of the paper) are promising organic molecules to study for organic water-splitting schemes. This hypothesis is based on their robust nature and strong visible-light absorption (they are relatively cheap, industrial dyes commonly used as colorants in

Received: December 6, 2013
Accepted: February 18, 2014
Published: March 24, 2014

car paints and plastics).[18] PDIs exhibit high thermal stability, with decomposition temperatures typically in the range of 300−600 °C,[19] and high oxidative stability in air and water, even resisting photobleaching in concentrated hypochlorite solutions.[20] Many PDIs exhibit a highest occupied molecular orbital (HOMO) that has a positive enough potential to oxidize water.[21] In the solid state, PDIs tend to π-stack, which often leads to a high degree of molecular order and strong electronic coupling between neighboring PDI molecules. Indeed, a polycrystalline PDI derivative has shown one of the longest exciton-transfer lengths (2.5 ± 0.5 μm) reported for an organic material.[22] These favorable properties have led several groups to propose the use of perylene derivatives in organic water oxidation systems.[8−10,23,24]

Herein we examine a water oxidation photoelectrochemical cell based on light absorption by a novel PDI derivative, N,N′-bis(phosphonomethyl)-3,4,9,10-perylenediimide (PMPDI), shown in Figure 1. A sub-hypothesis of this research is that

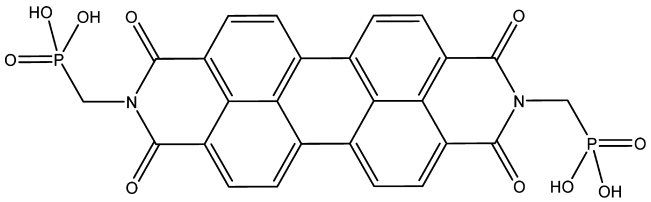

Figure 1. Structure of N,N′-bis(phosphonomethyl)-3,4,9,10-perylenediimide (PMPDI).

the phosphonate groups of PMPDI should be beneficial when coupling the dye with, specifically, a heterogeneous cobalt-oxide catalyst (CoO_x or Co-Pi)[25] which has been shown to have phosphate groups as a disordered component of its structure when electrochemically formed from phosphate-containing solutions.[26] We show herein that thin films of PMPDI on indium tin oxide (ITO) plus photoelectrochemically deposited[27] CoO_x (ITO/PMPDI/CoO_x) are capable of photo-assisted water oxidation with current densities in excess of 150 μA/cm^2 under a positive bias of 1.0 V vs. Ag/AgCl. We confirm the water-oxidation reaction through the direct detection of O_2, with a faradaic efficiency of 80 ± 15% under positive applied bias. We compare the performance of ITO/PMPDI/CoO_x anodes to those using another PDI derivative, N,N′-bis(1-ethylpropyl)-3,4,9,10-perylenediimide (EPPDI), as a way to probe the importance of phosphonate groups in the structure, the results of which do implicate a role for the phosphonate groups in PMPDI. Finally, we hypothesize about the performance-limiting factors of our current system and propose future directions for optimization of the system.

RESULTS AND DISCUSSION

Synthesis and Characterization of PMPDI. PMPDI was conveniently synthesized by adjusting a literature procedure[28] for an N,N′-bis(phosphono*ethyl*) PDI derivative. Specifically, PMPDI (Figure 1) was formed from the dehydration reaction between perylene tetracarboxylic dianhydride (PTCDA) and (aminomethyl)phosphonic acid in molten imidazole. The crude product was purified by two cycles of dissolving the product in water by deprotonating it to the tetra-potassium salt in basic solution, filtering out any remaining PTCDA, precipitating the product by adding acid until pH 1, then collecting the solid on a filter to separate it from residual imidazole dissolved in the acidic solution. The purified product was dried overnight in a vacuum oven, giving a 90% yield. The product was pure by proton and phosphorus NMR (see Figures S1 and S2 in the Supporting Information), although the proton NMR showed highly broadened peaks, especially for the aromatic protons. Peak broadening is commonly observed for PDIs and has been attributed to π-stacking aggregation.[28,29] HPLC showed evidence of trace PTCDA (see Figure S3 in the Supporting Information), though it is likely that this impurity was due to the slow hydrolysis of PMPDI under the basic chromatography conditions, not from remaining starting material. Mass spectrometry was used to confirm PMPDI by the identification of its mono- and di-deprotonated ions ($[M-H]^-$ and $[M-2H]^{2-}$, respectively). Elemental analysis of the product, as collected, was consistent with the monopotassium, dihydrate salt of PMPDI (K1-PMPDI·2H_2O).

Cyclic voltammetry of PMPDI (aq) was performed in pH 10 potassium carbonate buffer degassed with argon (Figure 2a). At

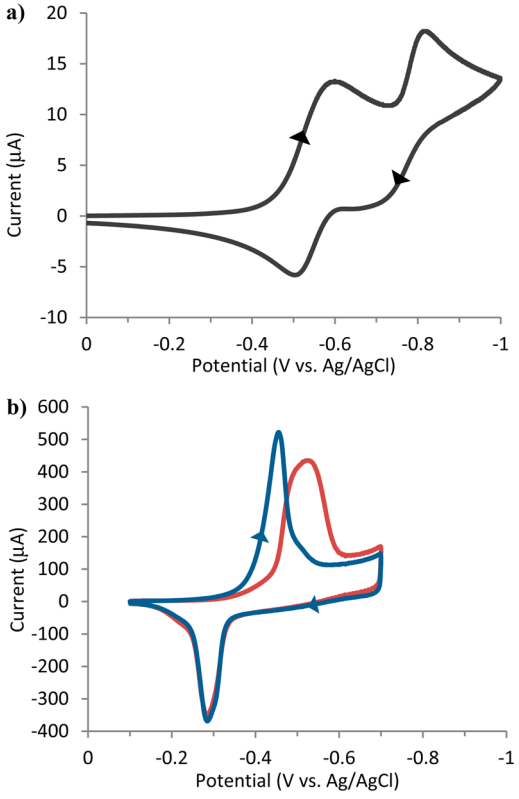

Figure 2. (a) CV of PMPDI dissolved in degassed 0.1 M carbonate buffer (pH 10) using a diamond working electrode, Pt wire counter electrode, Ag/AgCl reference, 50 mV/s scan rate. (b) CV of ITO/PMPDI electrode in degassed 0.1 M pH 7 potassium phosphate buffer, Pt wire counter electrode, Ag/AgCl reference, 50 mV/s scan rate, showing the first and second sweeps (red and blue lines, respectively).

this pH, PMPDI is actually the fully-deprotonated, $PMPDI^{4-}$ (see below). A boron-doped diamond working electrode was used for its low background currents in the scan region. Voltammetry was started at 0.0 V vs. Ag/AgCl and scanned in the negative direction. The voltammogram of $PMPDI^{4-}$ (aq) shows two reduction waves, typical of PDIs,[21] with the $E_{1/2}$ of the first reduction at −0.55 V, and the second at −0.78 V vs. Ag/AgCl. The second reductive wave shows less chemical reversibility than the first, and if dissolved oxygen is present in solution, both reduction waves become almost completely

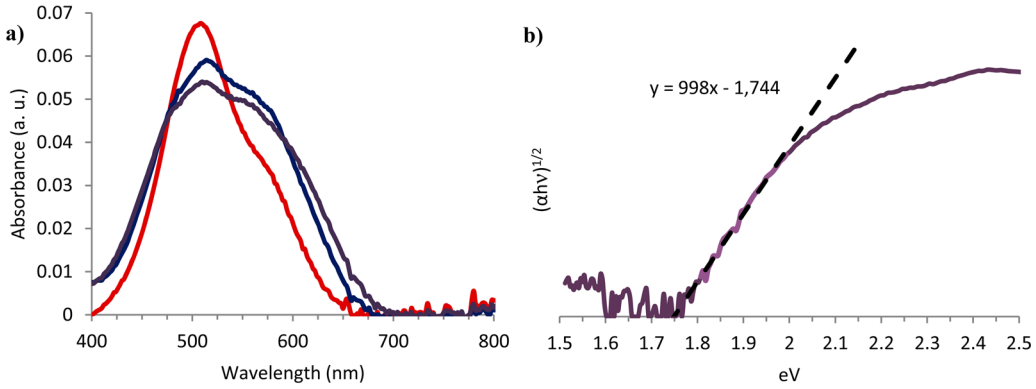

Figure 3. (a) Absorbance spectra of PMPDI thin films on ITO taken after spin coating from basic solution (red line), after dipping in acid solution (blue line) and after dipping in pH 7 KPi buffer (purple line). A clean ITO slide was used as background. (b) Tauc plot[38] of the KPi-rinsed film used to estimate the band gap (see the main text below).

chemically irreversible. This is as expected, due to the known reactivity of reduced PDIs with oxygen, even leading to their use as oxygen sensors.[30]

The oxidation potentials of PDIs cannot typically be determined in aqueous solutions, as their oxidation potential lies more positive than that of water.[31] Interestingly, we did see a catalytic oxidative wave for $PMPDI^{4-}$ (aq) on a boron-doped diamond electrode at potentials slightly negative of the background water oxidation (see Figure S4a in the Supporting Information). Bulk electrolysis experiments coupled with oxygen detection indicates that the majority of this oxidative current does not yield O_2 (see Figure S4a in the Supporting Information and the accompanying discussion). This indicates that the catalytic oxidative wave in the CV in Figure S4 in the Supporting Information may originate from the irreversible degradation of oxidized PMPDI or by some other PMPDI-catalyzed oxidation reaction that does not yield O_2. Even if these currents are caused by the degradation of PMPDI, this does not necessarily reflect the dye's oxidative stability under the photoelectrochemical conditions below when it is used as a water-oxidation photoanode, as these anodes have CoO_x catalyst present to help regenerate, and thus kinetically protect, any photo-oxidized dye.

Thin films of PMPDI were prepared by spin coating PMPDI from basic water solution onto cleaned ITO slides, then protonating the PMPDI by dipping the film in acidic solution to render it insoluble. X-ray photoelectron spectroscopy (XPS) was used to determine the C:K ratio in the films at various stages of preparation (see Figure S6 in the Supporting Information). The films, as spun from basic solutions, showed C:K ratios consistent with the tetrapotassium salt, K4-PMPDI. After submerging in acidic solution, no potassium was detected, consistent with the fully-protonated PMPDI. After submerging in pH 7 potassium phosphate (KPi) buffer, the C:K ratio was consistent with the dipotassium salt, K2-PMPDI.

Cyclic voltammetry was performed on the ITO/PMPDI films in 0.1 M pH 7 KPi buffer solution, in which the dye should be in the K2-PMPDI form. Similar to the dissolved, K4-PMPDI dye, K2-PMPDI films also show two reductive waves (see Figure S4b in the Supporting Information); however, the voltammogram does not show the behavior expected for an ideal nernstian reaction of a surface-confined film (i.e., where anodic and cathodic waves are mirror-images reflected across the potential axis, and where the peak anodic current and potential equals the peak cathodic current and potential).[32] Instead, the films showed significant chemical irreversibility (as indicated by unequal peak heights) and poor electrochemical reversibility (as indicated by a 170 mV offset in the peak potential between the anodic and cathodic waves at 50 mV/s scan rate). The chemical irreversibility is likely due to a combination of (1) reaction of reduced PMPDI with trace dissolved oxygen, and (2) loss of the twice-reduced dye from the film due to dissolution. Indeed, the chemical reversibility is greatly improved if the scan is reversed before the second reduction (Figure 2b). It should also be noted that the initial reduction wave of a virgin film is quite broad (red line, Figure 2b), but subsequent cycles consistently result in a sharper reduction wave which peaks at a less negative potential (blue line, Figure 2b). The peak potential of the reduction wave after the first sweep occurs at −0.46 V, while the subsequent reoxidation peak is shifted positive to −0.29 V vs. Ag/AgCl. Furthermore, the integrated charge under the reoxidation wave is only about half of that under the reduction wave. This behavior of significant potential shift between anodic and cathodic peaks has been reported previously for thin films of a liquid crystal PDI derivative.[31] In that case, the results were rationalized as a reversible molecular reorganization or phase change in the film as a result of the reduction or oxidation (likely as a result of counterions diffusing into or out of the film), causing the reverse electron-transfer process to occur at a different potential.[31]

When preparing PMPDI films, it was noted that after they are immersed in acid solution to protonate the phosphonate groups, the film tint visibly changes from red to a darker violet color. This change can be seen in the UV−vis as a broadening of the absorbance, especially in the longer wavelengths, as shown in Figure 3a. The absorbance broadens further after the films are submerged in pH 7 KPi solution (the electrolyte used for subsequent experiments). A similar color change was also observed in small isolated regions of PMPDI films that were left on the benchtop under ambient conditions for several weeks. Red and black phases have been reported for many PDI films,[33−36] forming both spontaneously and under solvent vapor annealing. These different phases are attributed to a slight shift in the π-stacking offset between neighboring perylene molecules, leading to a lower-energy intermolecular charge transfer transition.[36,37]

A Tauc plot can be used to estimate the optical band gap of amorphous thin film materials,[38] plotting $(\alpha h\nu)^{1/2}$ vs. the photon energy, $h\nu$, where α is the absorption coefficient, h is

Planck's constant, and ν is the photon frequency. The exponent of 1/2 is used for amorphous solids derived under the assumption that the density of states at the band edges have a parabolic shape.[38] The solid-state optical band gap of the KPi-rinsed PMPDI film was estimated by this method to be 1.75 eV (Figure 3b).

Construction of an Approximate Band Diagram. The electrochemical and optical information gathered for PMPDI can be used to estimate the energies of the HOMO and LUMO (or, more accurately, the valence band and conduction band, respectively, in the solid state) in order to generate an approximate band diagram for our system. Although the field of organic semiconductors and their applications are growing rapidly, there is not yet a consensus in the literature as to the best way of measuring their electronic energy levels.[39−41] The most direct methods are based on surface photoelectron spectroscopy,[41] which take measurement of solid films in a vacuum; however, approximations are also frequently made by measurement of electrochemical reduction and/or oxidation potentials, sometimes combined with measurements of the optical band gap.[40] The latter method was chosen for this study, since the electrochemical experiments are done on wet films suspended in electrolyte solution, nearly identical to the operating conditions of our final photoelectrochemical cell.

While the LUMO energy of PMPDI can be estimated from the $E_{1/2}$ of its first reductive wave when dissolved in solution, this LUMO energy is likely different from the conduction band edge of PMPDI films because of strong intermolecular interactions between nearest neighbors.[42] Therefore, the energy of the conduction band edge is likely best estimated by the reduction potential of PMPDI in the solid-state film. Unfortunately, the irreversibility of the ITO/PMPDI voltammograms shown in Figure 2b makes the precise determination of a formal reduction potential problematic; however, a rough estimation of the conduction band edge can be made from the average onset potential of the first reductive wave.[40] (The peak reduction potential would be a more straightforward estimation, but the peak potential shifts significantly with scan rate, as shown in Figure S5 in the Supporting Information.) The average onset potential for four voltammograms of different scan rates was −0.39 V vs. Ag/AgCl (see Figure S5 in the Supporting Information). Combining this value with the optical band gap of the PMPDI film as determined above, an *approximate* band diagram for our system is shown in Figure 4. Potentials of materials other than PMPDI are estimated as described below.

The work function of ITO under similar cleaning conditions has been reported as 4.40 eV vs. vacuum,[43] although the actual potential in most of the experiments in this study is the applied potential vs. Ag/AgCl from the potentiostat. The catalytic onset of water oxidation by CoO_x on an ITO electrode is reported as (and was confirmed by us at) 1.23 V vs. NHE in pH 7 KPi buffer.[25] By the Nernst equation, the potential of water oxidation is 0.82 V vs. NHE at pH 7. The above potentials can be reported relative to the Ag/AgCl reference electrode employed by the following relationships[32]

$$E_{\text{eV vs. vacuum}} - 4.5\ \text{eV} = eE_{\text{V vs. NHE}}$$

$$E_{\text{V vs NHE}} - 0.20\ \text{V} = E_{\text{V vs. Ag/AgCl}}$$

Importantly, it is clear from the band diagram in Figure 4 that photogenerated holes in the PMPDI film should have sufficient thermodynamic potential to oxidize water.

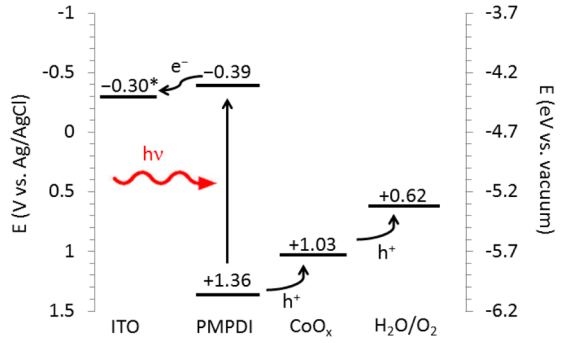

Figure 4. Band diagram for the ITO/PMPDI/CoO_x system. Estimated energy levels are given vs. Ag/AgCl; a secondary *y*-axis is shown vs. vacuum as an additional reference. Arrows indicate the absorption of light by the perylene layer, and the energy-storing transfer of indicated charge. *The actual potential of ITO in most experiments in this study is that applied via potentiostat vs. Ag/AgCl.

Photoelectrochemical Deposition of CoO_x Catalyst. Photoelectrochemical deposition of the catalyst was chosen since it has the advantage of preferentially depositing catalyst in areas where there is a high concentration of photogenerated holes.[17,44] Briefly, ITO/PMPDI anodes were immersed in 0.1 M pH 7 KPi buffer containing 1 mM $Co(NO_3)_2$. The catalyst was deposited at a potential of 700 mV vs. Ag/AgCl for 5 min while illuminated by a xenon arc lamp at approximately 100 mW/cm^2 intensity. Controls varying the process by using different cobalt concentrations, deposition times, and applied bias did not yield significantly different photo-assisted water-oxidation photocurrents. After depositing the catalyst, anodes were removed from cobalt solution and rinsed with DI water before further use. XPS spectra of PMPDI films were taken before and after the deposition in order to confirm that cobalt remains on the film after the catalyst deposition and a water rinse (see Figure S7a in the Supporting Information).

Photoelectrochemistry of ITO/PMPDI/CoO_x Anodes. Photocurrent transients vs. applied potential of an ITO/PMPDI/CoO_x anode in 0.1 M pH 7 KPi buffer are shown in Figure 5a. Importantly, practically no photocurrent (<1 μA/cm^2) is observed for bare ITO controls (blue line, Figure 5a, or Figure S10b in the Supporting Information for better scale), and relatively small photocurrents (<10 μA/cm^2) are observed for ITO/PMPDI controls (green line, Figure 5a, or Figure S10a in the Supporting Information for better scale). The origin of the photocurrent at ITO/PMPDI anodes is not known, but could possibly be due to photo-oxidation of trace impurities by PMPDI, low levels of water oxidation by PMPDI, or some destructive oxidation of PMPDI itself. When the CoO_x cocatalyst is present on ITO/PMPDI anodes, photocurrents grow ten-fold from about 15 μA/cm^2 at zero applied bias to over 150 μA/cm^2 at 1.0 V applied bias. At applied biases higher than 1.0 V vs. Ag/AgCl, oxidation currents begin to flow even in the dark (red line, Figure 5a).

The photocurrent transients of ITO/PMPDI/CoO_x anodes exhibit a spikelike behavior, with an initial peak in anodic current when the light is turned on. This indicates the generation of charge carriers from exciton dissociation, where electrons are collected at the ITO/PMPDI interface and holes are transferred to CoO_x at the opposite interface where they can then oxidize water. The initial photocurrent spike is followed by a gradual decay to a steady-state photocurrent, indicating that a fraction of the photogenerated holes are lost to

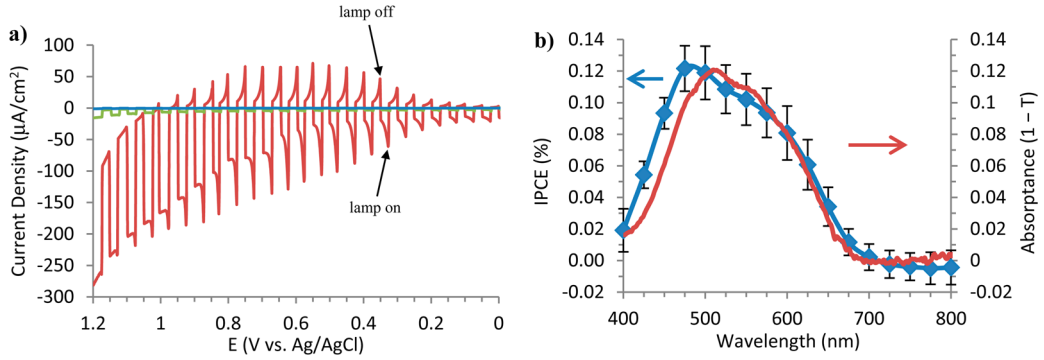

Figure 5. (a) Photocurrent transients vs. applied potential for ITO/PMPDI/CoO_x (red line), ITO/PMPDI (green line), and bare ITO (blue line), in 0.1 M pH 7 KPi buffer, 5 mV/s scan rate starting from 0.0 V (i.e., from right to left) with 5 s light transients. (b) average IPCE and standard deviation (blue squares and line) using a two-electrode configuration at short circuit in degassed 0.1 M pH 7 KPi buffer solution. The absorptance ($1 - T$) spectrum (red line) of a dry PMPDI film is overlaid for comparison.

bulk or surface recombination before they can contribute to the faradaic current.[45]

When the light is turned off, a reverse, cathodic current peaks and quickly decays to zero, indicating that recombination of the hole reservoir (i.e., the oxidized catalyst or water-oxidation intermediates at the surface) is competitive with the forward water-oxidation process. When a one-electron redox couple is added to the electrolyte solution, such as $Fe^{II}(CN)_6^{4-}$ (i.e., a kinetically more facile, one-electron redox reaction vs. the four-electron, two-water-molecule water-oxidation reaction), the cathodic spikes are greatly reduced, especially at lower potentials (see Figure S8 in the Supporting Information). Also, when no catalyst is present (i.e., the ITO/PMPDI control, Figure S10a in the Supporting Information) there are no cathodic current spikes when the light is turned off, consistent with the cathodic current being associated with the CoO_x catalyst.

It should be noted that many of the phenomena occurring during the photocurrent transient experiments (such as exciton dissociation efficiency, the amount of charge buildup, and all charge-transfer rate constants) are potential dependent. As the applied potential is increased, the peak anodic currents also increase, indicating that more holes are reaching the interface to oxidize water. This buildup of holes also leads to higher recombination currents, as indicated by the increasing dark, peak cathodic currents as the applied potential increases from 0 to 0.5 V vs. Ag/AgCl. At applied potentials positive of 0.5 V, the cathodic peaks begin to decrease despite the still-rising anodic peaks, indicating a decreasing rate of recombination, which then leads to the higher steady-state anodic photocurrents observed in Figure 5a.

As for the general stability of our anodes, they can be stored under ambient conditions for months, and still show comparable photocurrents when tested in a transient experiment as described above. Also, the photocurrents tend to increase slightly for freshly-prepared anodes after repeating such transient experiments.

Cell Efficiency Studies. A few diagnostic cell efficiencies[46] can help to determine the shortcomings of our ITO/PMPDI/CoO_x water-oxidation anodes. First, the incident photon-to-current conversion efficiency (IPCE), or external quantum efficiency, can be measured in a two-electrode configuration by a chronoamperometry experiment while holding the electrodes at short circuit. A device's IPCE is a measure of three fundamental processes: the efficiency of light absorption to create excitons (η_{abs}), the efficiency of charge dissociation and transport of those charge carriers to their respective interfaces (η_{trans}), and the efficiency of interfacial charge transfer (η_{int}).[46] The IPCE spectrum averaged for several ITO/PMPDI/CoO_x anodes is shown in Figure 5b. The absorptance ($1 - T$) spectrum of a dry PMPDI film (KPi-rinsed, K2-PMPDI) is shown for comparison, indicating that the photocurrents observed during these measurements coincide with absorption of light by PMPDI.

If all other processes were 100% efficient, a device's IPCE could only reach as high as its light harvesting efficiency (η_{abs}), that is, its absorptance spectrum. The low absorptance values measured for our ITO/PMPDI/CoO_x anodes (12% at the λ_{max}) indicate that light harvesting limitations are a major contributor to our low IPCE values. To investigate the other limitations to performance, a system's internal quantum efficiency, or absorbed photon-to-current conversion efficiency (APCE), can be calculated by dividing the IPCE values by the film's absorptance values at each wavelength. The APCE thus measures only the efficiencies of charge dissociation and transport, and the efficiency of interfacial charge transfer, η_{trans} and η_{int}, respectively.[46] By this treatment, our anodes typically show APCEs between 1 and 2%.

Finally, if the IPCE experiment is carried out with an added facile redox couple, and if η_{int} can be taken as ≈1, then the APCE should be a measure of only η_{trans}.[46] For our ITO/PMPDI/CoO_x anodes, we repeated the IPCE measurements with added $K_4Fe(CN)_6$ (a kinetically more facile, albeit one-electron, redox couple), which resulted in IPCE values that were generally double those without any $K_4Fe(CN)_6$ (see Figure S9 in the Supporting Information). The APCE values (which should reflect only the charge transport efficiency) were then estimated to be ~3% (assuming the efficiency of the interfacial hole transfer to $Fe^{II}(CN)_6^{4-}$ is ≈1; the control performed next suggests that it is actually <1).

As a control, we also ran an IPCE experiment with added hydroquinone, a two-electron, two-proton redox couple, a therefore closer model to the four-electron, four-proton water oxidation reaction. Interestingly, the IPCE values measured in the presence of hydroquinone are roughly double the values when $Fe^{II}(CN)_6^{4-}$ was used at the same concentration (~5 mM, see Figure S9 in the Supporting Information), giving APCE values of ~6%. As an additional control, we ran an IPCE with much more concentrated hydroquinone (200 mM), but the photocurrents were essentially unchanged. Therefore, with

the assumption that the η_{int} for hydroquinone is 1, then the estimated maximum η_{trans} in our ITO/PMPDI/CoO_x anodes is ~6%.

Preliminary Optimization Studies and Controls. Because the efficiency of light absorption is a major performance-limiting factor in our system, one key question to answer was whether or not our efficiencies could be improved by employing thicker PMPDI films to absorb more of the incident light. Attempts to alter the spin coating parameters employed to produce thicker films (e.g., lowering the spin rate) yielded only small changes in thickness. Thicker films, although not very uniform, were prepared by drop coating PMPDI solutions and letting the water slowly evaporate. A few of these films, roughly 3 times thicker than typical spin-coated films according to UV−vis, were used to prepare ITO/PMPDI/CoO_x anodes following the same standard procedures. Under photoelectrochemical testing, these thicker ITO/PMPDI/CoO_x anodes showed roughly one-tenth the steady-state photocurrents as our standard, thinner-film anodes (see Figure S10a in the Supporting Information).

The low dielectric constant of most organic materials causes excitons in such media to be strongly bound because of the coulombic attraction between electrons and holes. Therefore, excitons often must reach a materials interface in order to dissociate into separated charge carriers.[42] Exciton diffusion lengths in most organic materials are short (between 5 and 30 nm); hence, if films are prepared that are thicker than the exciton diffusion length, most excitons formed in the film bulk are expected to relax before reaching an interface to dissociate.[42] Through a combination of UV−vis and optical profilometry measurements, the absorption coefficient of PMPDI films (KPi rinsed, K2-PMPDI) was estimated at 2.0 × 10^4 cm^{-1} (see Figure S11 and its discussion in the Supporting Information). This absorption coefficient was used to determine that typical thicknesses of our spin-coated PMPDI films are 40−50 nm. The thicker, drop-cast films were then roughly 150 nm thick, and therefore about an order of magnitude thicker than typical exciton diffusion lengths. Therefore, it can be expected that the majority of excitons formed in these thicker films will relax before they can dissociate into useable charges.

To test the hypothesis that the phosphonate groups of PMPDI are important for the overall performance of the device, we also prepared anodes using another PDI derivative, EPPDI, with 1-ethylpropyl groups in the place of PMPDI's phosphonomethyl groups. The ITO/EPPDI films were prepared by spin-coating EPPDI from $CHCl_3$ solutions. Interestingly, these films remained a bright-red color upon submerging in aqueous solution (no black phase was observed). Regardless of film thickness, photocurrents during CoO_x catalyst depositions and subsequent photoelectrochemical testing were about an order of magnitude *smaller* than our typical ITO/PMPDI/CoO_x anodes (see Figure S10b in the Supporting Information). XPS spectra were collected both before and after catalyst deposition, and showed that only trace cobalt was present on the EPPDI films (see Figure S7b in the Supporting Information), which is further supported by the lack of any dark cathodic peaks during transient experiments (see Figure S10b in the Supporting Information), as such peaks were characteristic of the CoO_x catalyst on PMPDI films. These results are consistent with phosphonate groups being important for efficiently linking the CoO_x catalyst to the organic film; however, the results could also be explained by poor conductivity of the film, which could be caused by film morphology, poor interaction with the ITO substrate, or other unknown factors. Indeed, we found that EPPDI films did not adhere well to ITO, and often delaminated upon rinsing. Needed here is a systematic study of the photoelectrochemical properties of more PDI films, including testing derivatives with different functionalities (i.e., studies of dyes with and without phosphonate groups, but with otherwise similar structures) to see if PDI dyes with different functional groups are also capable of visible-light- and CoO_x-assisted water oxidation. Such studies are currently underway.

Evolved Oxygen Quantification. To confirm that photocurrents observed from the ITO/PMPDI/CoO_x anodes originate from oxidation of water and not from some other undesired process, it was necessary to directly quantify any photoelectrochemically produced O_2.[46] Previous studies have followed the concentration of oxygen in the headspace above solution in the photoelectrochemical cell,[25] or dissolved oxygen in the working electrolyte itself.[11,12,17] We chose the latter, well-established method for our studies due to the relatively small photocurrents produced by our anodes, and due to an observed gradual deactivation of our photoanodes over the five min time scale of water-oxidation experiments (see Figure S12 in the Supporting Information).

Details for oxygen quantification experiments are provided in the Experimental Section; attention to those details matter for anyone reproducing this work as it took on the order of 3 months of research to optimize, and then make, the O_2 yield measurements and controls reported herein. Briefly, a Clark-type electrode was used to measure the dissolved oxygen concentration in the working compartment solution both before and after a 5 min, illuminated, amperometric water-oxidation experiment. The change in dissolved oxygen concentration and the known volume of solution in the working compartment were used to calculate the number of micromoles of oxygen produced. By recording the amount of current passed during the 5 min water oxidation, and using the stoichiometry for the water-oxidation reaction ($2H_2O \rightarrow 4H^+ + O_2 + 4e^-$), the theoretical yield for a perfect faradaic reaction can be calculated as

$$\left(\frac{6.241 \times 10^{18}\ e^-}{1\ \text{Coulomb}}\right)\left(\frac{1\ \text{molecule}\ O_2}{4\ e^-}\right)\left(\frac{1\ \text{mol}}{6.022 \times 10^{23}\ \text{molecules}}\right)\left(\frac{1 \times 10^6\ \mu\text{mol}}{1\ \text{mol}}\right)$$

$$= 2.591\ \mu\text{mol}\ O_2/\text{Coulomb passed}$$

Then, the faradaic efficiency was calculated by dividing the measured oxygen yield by the theoretical yield.

The literature reports that ITO/CoO_x has a faradaic efficiency of 100% in 0.1 M KPi buffer at pH 7, with an applied bias of 1.1 V vs. Ag/AgCl.[25] Several controls were done in order to both verify the literature result in our hands and to check our multipoint calibration. First, ITO/CoO_x anodes were prepared as published,[25] except that a more concentrated Co^{2+} solution was used (1 mM vs. 0.5 mM) and the deposition was stopped after 5 min (depositing less catalyst) in order to closely mimic our conditions for CoO_x formation on ITO/PMPDI. The ITO/CoO_x anodes thus prepared were used for a 5 min amperometric water-oxidation experiment held at or below 1.1 V vs. Ag/AgCl (slightly lowering the potential decreases currents to more closely parallel the currents in the ITO/

PMPDI/CoO_x systems) and under both illuminated and dark conditions (ITO/CoO_x anodes have little light absorption in the visible, and therefore exhibit no additional photocurrent; however, these controls provided confidence in our Clark electrode calibration concerning temperature changes in solution caused by illumination). Results of 17 ITO/CoO_x water-oxidation control experiments, both dark and illuminated, resulted in an average faradaic efficiency of 100 ± 14%. These controls provide confidence in the method used for oxygen detection and its accuracy.

Finally, the same method was used to determine the faradaic efficiency for our ITO/PMPDI/CoO_x anodes held at 900 mV vs. Ag/AgCl and under illumination. Nine anodes yielded an average faradaic efficiency of 80 ± 15%, near the theoretical limit of 100% within our experimental error. Of course, it cannot be ruled out that other oxidative side reactions may be occurring, such as oxidation of trace impurities, degradative oxidation of PMPDI, or the formation of other water-oxidation products, such as hydrogen peroxide. Controls of ITO/PMPDI films without the CoO_x catalyst yielded no detectable oxygen, even when illuminated and held at 900 mV positive bias vs. Ag/AgCl. Overall, the results are quite pleasing in that a high, 80 ± 15% faradaic efficiency for water oxidation was achieved with our novel ITO/PMPDI/CoO_x system developed and studied herein. Further study of PDI-based photoelectrochemical water oxidation systems and their optimization and longer-term stability studies are, therefore, of interest in our opinion.

CONCLUSION

Although other perylene derivatives have been studied as components in organic bi-(or tri-)layer PV and water-oxidation devices,[8−10] the current study is, to our knowledge, the first device to achieve photochemically-driven water oxidation by a single-layer molecular organic semiconductor thin film coupled to a water-oxidation catalyst. Our comparison with anodes using another PDI dye, ITO/EPPDI/CoO_x yielded much lower performance. This indicates that the phosphonate groups found in PMPDI *may* be important for close electronic coupling between PMPDI and the CoO_x catalyst, but continued studies of other PDI derivatives will be required to further support or refute this hypothesis, and are currently under investigation.

It is important to note that the photocurrent densities generated by our ITO/PMPDI/CoO_x anodes, just over 150 $\mu A/cm^2$ at 1.0 V applied bias vs. Ag/AgCl, are small relative to many photoelectrochemical water-oxidation cells based on inorganic semiconductors.[5−7] However, our observed current densities are quite comparable to those achieved using other organic semiconductors,[8,9,11,12,17] despite ours being a largely unoptimized system. Current transient experiments revealed that the rate of recombination between holes in the oxidized catalyst and conduction band electrons is competitive with the desired water-oxidation reaction. While improvements can be expected for the current system through the use of a faster water-oxidation catalyst, such catalysts are generally composed of less earth-abundant, more expensive metals than cobalt (i.e., iridium or ruthenium). We can, however, expect that at least some improvement in the performance of our current system by the use of different interfacial layer material to enhance charge separation and prevent recombination between ITO and the perylene film. Such interfacial layers may also help to reduce the large applied bias required in our current system to reach its maximum photocurrents, given that the estimated HOMO of PMPDI should have more than sufficient overpotential to oxidize water (Figure 4).

Efficiency measurements of our system reveal that our anodes only reach a maximum IPCE of 0.12%. APCE calculations show that light absorption is a large limitation. Our PMPDI thin films are optically quite thin, absorbing only about 12% of incident light at the maximum absorbance. IPCE experiments with added hydroquinone allowed us to estimate the internal charge transport efficiency at 6%. Anodes with thicker PMPDI films which absorbed more of the incident light showed lower photocurrents, likely limited therefore by exciton diffusion lengths. We can still hope to improve our overall anode efficiency by employing a dye-sensitized mesoporous semiconductor architecture, where more light can be absorbed due to the high surface area of the semiconductor, while keeping the dye thickness to a monolayer, thereby eliminating the need for lengthy exciton diffusion. Those needed studies are also in progress.

We are currently in the process of synthesizing and testing other PDI derivatives in order to further test the hypothesis that phosphonate or other ionic groups are important structural components for coupling with the inorganic catalyst; those additional PDI derivatives will also probe if device stability can be improved by the choice of especially the most oxidation resistant PDIs. Of particular interest are lifetime studies which push the limit of a more optimized device, while also characterizing any deactivated device and system to understand its limitations (i.e., in light of the gradual drop in photocurrent we see, Figure S12 in the Supporting Information, which raises questions about the stability of the current PMPDI dye employed under extended photoelectrolysis conditions).

In summary, a novel perylene diimide derivative, PMPDI, was successfully synthesized and characterized. This dye is conveniently soluble in basic solutions and insoluble in neutral and acid solutions, allowing for solution-based processing. PMPDI absorbs strongly in the visible and has electronic energy levels conducive to water oxidation. We have preliminary evidence that the phosphonate groups of PMPDI may be a critical component to effectively couple the CoO_x catalyst to the organic dye. It has been confirmed that PMPDI thin films, spin-coated from solution onto ITO, can achieve photo-assisted water oxidation when coupled with photoelectrochemically deposited CoO_x catalyst. Our IPCE results confirm that photocurrents generated by the ITO/PMPDI/CoO_x electrodes originate from PMPDI absorption of light, and water oxidation has been confirmed by the direct detection of O_2, with a faradaic efficiency of 80 ± 15% under positive applied bias. Additional studies of other PDI dyes, of nanostructured versions of our device, of the stability of those second-generation devices, and of the kinetics of the photoelectrocatalysis are in progress and will be reported in due course.

EXPERIMENTAL SECTION

Materials. Perylene-3,4,9,10-tetracarboxylic dianhydride (PTCDA) (97%, Aldrich), (aminomethyl)phosphonic acid (99%, Alfa Aesar), and imidazole (99%, Acros Organics) were all used as received. N,N′-bis(1-ethylpropyl)-3,4,9,10-perylenediimide (EPPDI) was synthesized according to the literature.[47] Characterization data can be found at the end of the Supporting Information. One-inch-square indium tin oxide (ITO) glass slides were purchased from Delta Technologies and cleaned before use (see below). Solvents were purchased from Sigma-Aldrich or Fisher Scientific and used without further purification.

Ultrapure water (18 MΩ) was used for all cleaning steps and for preparation of electrochemical solutions.

Synthesis of N,N′-bis(phosphonomethyl)-3,4,9,10-perylenediimide (PMPDI). The synthesis of PMPDI was modified from a literature procedure[28] for the N,N′-bis(phosphono*ethyl*) PDI derivative. A mixture of PTCDA (79 mg, 0.20 mmol), (aminomethyl)-phosphonic acid (47 mg, 0.42 mmol), and 1.5 g of imidazole were added to a 25 mL round-bottomed flask with a magnetic stir bar. The flask was sealed with a rubber septum to prevent evaporative loss of imidazole and lowered into a hot oil bath at 130 °C (venting briefly as the flask contents warmed). After stirring for 20 min in the oil bath, the flask was removed and allowed to cool for approximately 2 min before 5 mL of a 50/50 vol% mixture of 2 M HCl/ethanol was added to precipitate a fine black solid. The solid was collected on a nylon, 0.22 μm vacuum filter and rinsed with 5 mL each of 50/50 water/ethanol, then ethanol. This product (an imidazolium salt by ^{1}H-NMR) was suspended in 10 mL of DI water and dissolved by the dropwise addition of 1 M KOH (the solid began to dissolve at pH ∼8 and was completely dissolved by pH 9.5). The solution was then vacuum-filtered to remove any unreacted PTCDA. (Note: if the solution is made too basic, the PTCDA will dissolve as well and will not be separated from the product.) The filtrate was then acidified by the dropwise addition of 2 M HCl while under rapid magnetic stirring. (Note: the product precipitates in bulk at approximately pH 5.5, forming a gel, likely as the dipotassium salt. More acidic conditions are required to remove imidazole impurities, and further stirring and dilution helps liquefy the gel before filtering.) The mixture was brought to pH ∼1, and the precipitated product was collected by vacuum filtration. NMR of this product usually contained trace imidazole, but can be purified by repeating the dissolving and precipitation procedure, giving a 90% yield after drying overnight in a vacuum oven at 100 °C. Elemental analysis of the product, as collected, was consistent with the mono-potassium, dihydrate of PMPDI, indicating that the product kinetically precipitates as the mono-potassium salt, which was used for subsequent studies. The fully protonated product was also obtained by dissolving the solid in NaOH solution and leaving the solution to slowly acidify for 24 h in a desiccator saturated with HCl vapor. FT-IR (Nicolet SX-60 FT-IR spectrometer with ATR-ZnSe): 3403 cm^{-1} br m, 3067 w, 3000 w, 2948 w, 1690 s, 1650 s, 1589 s, 1575 m, 1506 w, 1485 w, 1435 m, 1402 w, 1392 m, 1363 m, 1335 m, 1301 m, 1248 m, 1186 w, 1162 w, 1106 w, 970 w, 928 br m, 861 w, 843 w, 809 w, 792 w, 733 w, 708 w. Samples for NMR (300 MHz Varian Inova) were dissolved by sonication in D_2O with half a drop of 30% NaOD (in D_2O). ^{1}H-NMR, δ (ppm): 7.85 (br, 8H, Ar); 4.16 (br, 4H, N−CH_2−P) (see Figure S1 in the Supporting Information). ^{31}P-NMR, δ (ppm): 12.15 ppm (see Figure S2 in the Supporting Information). MS (ESI/APCI in NH_4OH matrix): m/z calculated for PMPDI ($C_{26}H_{16}N_2O_{10}P_2$) = 578.03, found m/z = 577.02 $[M-H]^-$; 288.01 $[M-2H]^{2-}$. Elemental analysis of the fully-protonated product, calculated for $C_{26}H_{16}N_2O_{10}P_2$ (found): 53.99% C (51.97); 2.79% H (3.17); 4.84% N (4.80); 0% Na (0.194). The product was also analyzed by HPLC (see Figure S3 in the Supporting Information) and cyclic voltammetry (Figure 2a and Figure S4a in the Supporting Information).

ITO/PMPDI/CoO_x Photoanode Preparation. ITO slides were cleaned by sonication for 30 min in a Liquinox surfactant solution, rinsed with water, then sonicated for 30 min each in acetone and isopropanol solutions and allowed to dry under ambient air for at least half an hour. Before use, slides were air-plasma treated (Harrick PDC-3XG) for 15 min and moved directly into a spin coater (SCS G3P-8 Spin Coater). The phosphonate groups of PMDPI make it conveniently soluble in water at pH ≥ 9.5 as the tetra-potassium salt. PMPDI solutions were prepared by adding 5 mg of PMPDI product (K1-PMPDI·$2H_2O$) to 1 mL of water and 2 drops of 1 M KOH, and sonicated to fully dissolve. These solutions were dripped through a 0.2 μm filter to cover the surface of a freshly cleaned one-inch square ITO substrate and spin-coated at 1000 rpm for 60 s. Dye was wiped from one edge of the slide by a wet Kimwipe in order to provide a naked ITO surface to attach copper tape as an electrical contact. These ITO/PMPDI slides were scored with a glass cutting tool and cleaved into two or three segments for further testing (typical active areas were 1−1.5 cm^2). The slides were then submerged for 30 s each in 20 mL of a 50/50 mixture of 2 M HCl/ethanol (fully protonating the PMPDI film and rendering it insoluble), distilled water, ethanol, and then blown dry under an argon stream for about a minute. Films were characterized at this point (before depositing catalyst) by UV−vis spectroscopy and cyclic voltammetry (see below). Before depositing CoO_x catalyst, a fingernail topcoat was used to cover the slide edges and any uncoated portions of the ITO surface to ensure that the only conductive surface in contact with solution was the PMPDI film. After the fingernail polish had dried, catalyst was deposited by submerging the active area of the ITO/PMPDI anode in a glass vial containing 10 mL of 0.1 M pH 7 KPi containing 1 mM $Co(NO_3)_2$, applying a potential of 700 mV vs. Ag/AgCl, and illuminating the anode for 5 min by a 65 W xenon arc lamp focused to approximately 100 mW/cm^2 intensity (measured with a Thorlabs Thermal Power Sensor Model S302A). Anodes were then removed from the cobalt solution, rinsed with DI water, and used for further testing. The presence of cobalt on rinsed and dried ITO/PMPDI/CoO_x anodes was confirmed by XPS (see below, and Figure S7 in the Supporting Information).

Thicker PMPDI films were also prepared by drop coating two (or more) drops of the above PMPDI solutions onto cleaned ITO slides, covering with a petri dish to protect from dust, and letting them air dry on a rotary table (Thermo Scientific Lab-Line Maxi Rotator). Such films did not evaporate evenly and created films of nonuniform thicknesses. These films were used to estimate the solid-state absorption coefficient as described in the Supporting Information, Figure S11. A few drop-coated films (roughly 3 times thicker than spin-coated films according to UV−vis) were tested for their photoelectrochemical performance. These films were processed and catalyst deposited under the same procedures as described above, and submitted to the same photoelectrochemical testing as described below. Resulting transients can be seen in Figure S10a in the Supporting Information.

ITO/EPPDI/CoO_x Photoanode Preparation. Photoanodes were prepared as described above, except spin coating was done from $CHCl_3$ solution, still at 1000 rpm for 60 s. Using the same dye concentrations as above (5 mg/mL), films spun from $CHCl_3$ were roughly 10 times the thickness of standard PMPDI films, as estimated by UV-Vis. Thinner films, comparable to the thickness of spin-coated PMPDI films, were also prepared by reducing dye concentrations to 1 mg/mL. EPPDI films stayed bright-red upon submersion into KPi solutions (no change to a black phase was observed). Cobalt catalyst was deposited under the same conditions described above. XPS was performed on one of the films after catalyst deposition, showing that only trace cobalt remained (see Figure S7b in the Supporting Information). ITO/EPPDI/CoO_x anodes were then submitted to the same photoelectrochemical testing as described below. Resulting transients can be seen in Figure S10b in the Supporting Information. Film thickness did not significantly alter the observed photocurrents.

XPS. Spectra were taken on a PHI 5800 XPS with Al Kα source at 350 W power, and analyzed using PHI MultiPak software. Samples were prepared by spin coating PMPDI onto ITO slides as described above. Slides were scored and broken into 3 pieces. The first was untreated after coating, a second was submerged in 20 mL of 50/50 2 M HCl/ethanol for 60 s, then rinsed by dipping several times in DI water then ethanol, and drying for a minute under an argon stream. The third piece was treated identically to the second, then also submerged for 60 s in 0.1 M pH 7 KPi buffer and rinsed again as above. These slides were allowed to dry overnight, and then analyzed by XPS, taking both a survey scan and a high resolution scan in the region of 280 to 305 eV to calculate the C:K ratio (see Figure S6 in the Supporting Information). This experiment was performed 3 times and the average C:K ratios were consistent with K4-PMPDI as coated, PMPDI after acid treatment, and K2-PMPDI after KPi treatment. XPS was also taken of PMPDI and EPPDI films both before and after a standard CoO_x catalyst deposition (see Figure S7 in the Supporting Information).

UV−vis. UV−vis data were collected by a Hewlett Packard 8452A diode array spectrophotometer. ITO/PMPDI slides were scored and broken into 1-cm-wide slices to fit into the sample holder and pressed against the back wall for consistent sample placement. An ITO slide, cleaned under the standard conditions (and spin coated with ∼0.05 M KOH as a control for the basic dye solution) was used as the reference blank.

Cyclic Voltammetry. Electrochemical experiments were performed on a CH Instruments CHI630D potentiostat using a platinum wire counter electrode and Ag/AgCl (sat. KCl) reference electrode. The potential of the Ag/AgCl reference was confirmed to be +0.20 V vs. NHE by a 1 mM $Fe(CN)_6^{3-/4-}$ in 0.1 M HCl reference redox system.[32] Cyclic voltammetry was performed on PMPDI both dissolved in basic solution ($PMPDI^{4-}$) and as a thin film on ITO in neutral solution (K2-PMPDI). For the aqueous PMDPI experiments, a solution of ∼4 mM PMPDI in 0.1 M pH 10 potassium carbonate buffer was degassed with argon before testing to avoid interference due to reduction of oxygen by reduced PMPDI or at the working electrode itself (3 mm boron-doped diamond (CCL Diamond)). Voltammograms of K2-PMPDI films on ITO were performed in degassed 0.1 M pH 7 KPi buffer.

Photoelectrochemical Testing. All photoelectrochemical experiments were performed in a custom-made two-compartment photoelectrochemical cell, with a working compartment made from 1 × 1.5 cm^2 quartz rectangular tubing with a working volume of 5 mL. The ITO/PMPDI/CoO_x anodes were pressed against the front wall of the cell (the glass back of the anode against the glass cell wall)and illuminated through the ITO-side with a 65 W xenon arc lamp (PTO model A 1010) powered by an OLIS XL150 adjustable power supply. The lamp was focused onto the cell through a bandpass filter (315−710 nm, Thorlabs FGS900S) to more closely simulate the AM1.5 solar spectrum, with an incident power density measured to be approximately 100 mW/cm^2, measured with a Thorlabs Thermal Power Sensor, model S302A. Photoelectrochemical experiments were recorded with the same potentiostat and electrodes as described above for cyclic voltammetry. Transient light experiments were performed by manually chopping the light source every 5 s using an opaque sheet of construction paper, while the applied potential was scanned from low to high values. Photocurrent densities tended to improve slightly upon repeating the transient experiment.

Action spectra were collected on a separate PV testing apparatus provided by Prof. C. M. Elliott's research group, which consisted of a xenon arc lamp (Oriel model 66002, 100 mW/cm^2), power supply (Oriel model 68700), monochrometer (Oriel Cornerstone 130, model 7400), and a Kiethley 2400 source meter. For these experiments, a two-electrode setup was used (ITO/PMPDI/CoO_x working electrode and Pt wire counter electrode) in the same two-compartment photoelectrochemical cell described above, containing degassed 0.1 M pH 7 KPi buffer (5 mL in the working compartment, 3 mL in the auxiliary compartment). The face of the cell was pressed against an aperture, leaving an illuminated area of 0.385 cm^2. To collect the action spectrum, the electrodes were held at short circuit while the incident light was scanned from 400 to 700 nm (≈10 nm bandwidth) in 25 nm steps, recording the steady-state current between the electrodes 15 s after each wavelength step. The incident lamp power at each wavelength step was recorded using a Thorlabs silicon standard power sensor, model S120B, in order to calculate the final IPCE values.

Oxygen Detection. Due to the relatively small photocurrents and gradual deactivation of our ITO/PMPDI/CoO_x anodes, dissolved oxygen concentration was directly detected in the KPi buffer solution instead of detecting O_2 in the headspace of the cell (consistent with this, the oxygen produced was not sufficient to generate visible bubbles). Dissolved oxygen was measured using a Clark-type electrode and meter (Microelectrodes, Inc., model M1-730A electrode and OM-4 oxygen meter), and recorded on LabView software. The Clark electrode was calibrated daily in two standard solutions of 0% (≥0.1 M Na_2SO_3)[48] and 20.9% (vortexed under ambient air) oxygen solutions—which corresponds to 0 μM and 236 μM dissolved oxygen, respectively, at 20 °C, correcting for the atmospheric pressure in Fort Collins, CO (typically between 83.2 and 85.6 kPa).[49] Because the working solution is heated by the lamp irradiation and because the Clark electrode response is temperature sensitive, the response was calibrated in both standard solutions over a temperature range of 20−30 °C (see Figure S13 in the Supporting Information for a typical calibration).

Water-oxidation experiments for our anodes were carried out using the same photoelectrochemical setup as described above. For these experiments, the lamp intensity was increased to ∼300 mW/cm^2 and an applied bias of 900 mV vs. Ag/AgCl was used in order to maximize the photocurrent, and thus the resultant oxygen production, yet stay below the potential at which PMPDI films showed dark oxidative currents (see Figure S4b in the Supporting Information). To avoid the difficulties of sealing the electrochemical cell from the atmosphere, we air-saturated solutions to begin with (i.e., vortexed under ambient air for at least 10 min). This way, any increase in dissolved oxygen concentration had to come from water oxidation and not from the surrounding air. The Clark electrode response in the 5 mL volume of solution in the working compartment and the temperature of solution (± 0.1 °C) were recorded both before and after a 5 min, illuminated, amperometric water-oxidation experiment. The solution was stirred only while measuring oxygen, and then only fast enough to yield a maximum electrode response. The calibration curve was used to convert the Clark electrode responses and temperatures to their corresponding oxygen concentrations. The volume of solution and change in concentration after the electrolysis was used to calculate the number of moles of oxygen produced. Finally, the current passed during the water oxidation was used to calculate the theoretical oxygen yield and the faradaic efficiency of the reaction.

It is important to note here that water oxidation and rising solution temperatures (due to high intensity illumination) resulted in solutions with dissolved oxygen concentrations above the equilibrium value. Controls were done by bubbling 100% oxygen into air-saturated solutions, creating slightly supersaturated conditions. Oxygen concentration was then monitored as a function of time and stir rate, confirming that the oxygen produced during electrolysis remained primarily in solution and did not escape to the atmosphere over the 5 min time scale of the experiments, at least to within the observed ±15% O_2-yield error bars.

■ ASSOCIATED CONTENT

Ⓢ Supporting Information

Characterization data for PMPDI: ^1H NMR, ^{31}P NMR, HPLC, cyclic voltammetry; XPS of PMPDI films and EPPDI films before and after CoO_x catalyst deposition; photocurrent transients and IPCE values for ITO/PMPDI/CoO_x anodes with and without added $Fe(CN)_6^{4-}$ or hydroquinone; photocurrent transients for ITO/PMPDI(thick film)/CoO_x and ITO/EPPDI/CoOx anodes; PMPDI absorption coefficient estimation by UV-Vis and optical profilometry; photocurrent decay during extended photoelecctrolysis; example Clark electrode calibration for oxygen detection; characterization data for EPPDI. This material is available free of charge via the Internet at http://pubs.acs.org.

■ AUTHOR INFORMATION

Corresponding Authors

*E-mail: brian.gregg@nrel.gov.
*E-mail: rfinke@lamar.colostate.edu.

Author Contributions

The initial draft of the manuscript was written by the first author. All authors have given approval to the final version of the manuscript.

Notes

The authors declare no competing financial interest.

■ ACKNOWLEDGMENTS

This research was supported in part by an award to J.J.S. from the Department of Energy, Office of Science, Graduate Fellowship Program, which was made possible in part by the American Recovery and Reinvestment Act of 2009 and is administered for the Department of Energy by the Oak Ridge Institute for Science and Education, managed by Oak Ridge Associated Universities under DOE Contract DE-AC05-06OR23100. This work was supported in part at the National Renewable Energy Laboratory (NREL) by the U.S. Department of Energy, Office of Science, Basic Energy Science, Division of Chemical Sciences, Geosciences and Biosciences, under Contract DE-AC36-08GO28308. This work was performed primarily at Colorado State University when it was supported by NSF Grant CHE-1057723 (to R.G.F.). We thank Prof. C.M. Elliott and his research group for helpful discussion and for the use of their photovoltaic testing apparatus.

■ ABBREVIATIONS

PDI, perylene diimide
PMPDI, N,N′-bis(phosphonomethyl)-3,4,9,10-perylenediimide
ITO, indium tin oxide
K1-PMPDI, monopotassium salt of PMPDI
K2-PMPDI, dipotassium salt of PMPDI
K4-PMPDI, tetrapotassium salt of PMPDI
EPPDI, N,N′-bis(1-ethylpropyl)-3,4,9,10-perylenediimide
PTCDA, perylene tetracarboxylic dianhydride
HOMO, highest occupied molecular orbital
LUMO, lowest unoccupied molecular orbital
KPi, potassium phosphate
XPS, X-ray photoelectron spectroscopy
IPCE, incident photon-to-current conversion efficiency
APCE, absorbed photon-to-current conversion efficiency

■ REFERENCES

(1) Lewis, N. S.; Nocera, D. G. Powering the Planet: Chemical Challenges in Solar Energy Utilization. *Proc. Natl. Acad. Sci. U.S.A.* **2006**, *103*, 15729−15735.
(2) Bard, A. J.; Whitesides, G. M.; Zare, R. N.; McLafferty, F. W. Holy Grails of Chemistry. *Acc. Chem. Res.* **1995**, *28*, 91.
(3) Bard, A. J.; Fox, M. A. Artificial Photosynthesis: Solar Splitting of Water to Hydrogen and Oxygen. *Acc. Chem. Res.* **1995**, *28*, 141−145.
(4) Fujishima, A.; Honda, K. Electrochemical Photolysis of Water at a Semiconductor Electrode. *Nature* **1972**, *238*, 37−38.
(5) Aharon-Shalom, E.; Heller, A. Efficient p-InP (Rh-H Alloy) and p-InP (Re-H Alloy) Hydrogen Evolving Photocathodes. *J. Electrochem. Soc.* **1982**, *129*, 2865−2866.
(6) Khaselev, O.; Turner, J. A. A Monolithic Photovoltaic-Photoelectrochemical Device for Hydrogen Production Via Water Splitting. *Science* **1998**, *280*, 425−427.
(7) Licht, S.; Wang, B.; Mukerji, S.; Soga, T.; Umeno, M.; Tributsch, H. Over 18% Solar Energy Conversion to Generation of Hydrogen Fuel; Theory and Experiment for Efficient Solar Water Splitting. *Int. J. Hydrogen Energy* **2001**, *26*, 653−659.
(8) Abe, T.; Nagai, K.; Ogiwara, T.; Ogasawara, S.; Kaneko, M.; Tajiri, A.; Norimatsu, T. Wide Visible Light-Induced Dioxygen Evolution at an Organic Photoanode Coated with a Noble Metal Oxide Catalyst. *J. Electroanal. Chem.* **2006**, *587*, 127−132.
(9) Abe, T.; Nagai, K.; Kabutomori, S.; Kaneko, M.; Tajiri, A.; Norimatsu, T. An Organic Photoelectrode Working in the Water Phase: Visible-Light-Induced Dioxygen Evolution by a Perylene Derivative/Cobalt Phthalocyanine Bilayer. *Angew. Chem., Int. Ed.* **2006**, *45*, 2778−2781.
(10) Liu, G.; Chen, C.; Ji, H.; Ma, W.; Zhao, J. Photo-Electrochemical Water Splitting System with Three-Layer n-Type Organic Semiconductor Film as Photoanode under Visible Irradiation. *Sci. China: Chem.* **2012**, *55*, 1953−1958.
(11) Youngblood, W. J.; Lee, S.-H. A.; Kobayashi, Y.; Hernandez-Pagan, E. A.; Hoertz, P. G.; Moore, T. A.; Moore, A. L.; Gust, D.; Mallouk, T. E. Photoassisted Overall Water Splitting in a Visible Light-Absorbing Dye-Sensitized Photoelectrochemical Cell. *J. Am. Chem. Soc.* **2009**, *131*, 926−927.
(12) Brimblecombe, R.; Koo, A.; Dismukes, G. C.; Swiegers, G. F.; Spiccia, L. Solar Driven Water Oxidation by a Bioinspired Manganese Molecular Catalyst. *J. Am. Chem. Soc.* **2010**, *132*, 2892−2894.
(13) Moore, G. F.; Blakemore, J. D.; Milot, R. L.; Hull, J. F.; Song, H.; Cai, L.; Schmuttenmaer, C. A.; Crabtree, R. H.; Brudvig, G. W. A Visible Light Water-Splitting Cell with a Photoanode Formed by Codeposition of a High-Potential Porphyrin and an Iridium Water-Oxidation Catalyst. *Energy Environ. Sci.* **2011**, *4*, 2389−2392.
(14) Zhao, Y.; Swierk, J. R.; Megiatto, J. D.; Sherman, B.; Youngblood, W. J.; Qin, D.; Lentz, D. M.; Moore, A. L.; Moore, T. A.; Gust, D.; Mallouk, T. E. Improving the Efficiency of Water Splitting in Dye-Sensitized Solar Cells by Using a Biomimetic Electron Transfer Mediator. *Proc. Natl. Acad. Sci. U.S.A.* **2012**, *109*, 15612−15616.
(15) Gao, Y.; Ding, X.; Liu, J.; Wang, L.; Lu, Z.; Li, L.; Sun, L. Visible Light Driven Water Splitting in a Molecular Device with Unprecedentedly High Photocurrent Density. *J. Am. Chem. Soc.* **2013**, *135*, 4219−4222.
(16) Alibabaei, L.; Brennaman, M. K.; Norris, M. R.; Kalanyan, B.; Song, W.; Losego, M. D.; Concepcion, J. J.; Binstead, R. A.; Parsons, G. N.; Meyer, T. J. Solar Water Splitting in a Molecular Photoelectrochemical Cell. *Proc. Natl. Acad. Sci. U.S.A.* **2013**, *110*, 20008−20013.
(17) Bledowski, M.; Wang, L.; Ramakrishnan, A.; Bétard, A.; Khavryuchenko, O. V.; Beranek, R. Visible-Light Photooxidation of Water to Oxygen at Hybrid TiO_2−Polyheptazine Photoanodes with Photodeposited Co-Pi (CoO_x) Cocatalyst. *ChemPhysChem* **2012**, *13*, 3018−3024.
(18) Law, K. Y. Organic Photoconductive Materials: Recent Trends and Developments. *Chem. Rev.* **1993**, *93*, 449−486.
(19) Pasaogullari, N.; Icil, H.; Demuth, M. Symmetrical and Unsymmetrical Perylene Diimides: Their Synthesis, Photophysical and Electrochemical Properties. *Dyes Pigm.* **2006**, *69*, 118−127.
(20) Langhals, H. Cyclic Carboxylic Imide Structures as Structure Elements of High Stability. Novel Developments in Perylene Dye Chemistry. *Heterocycles* **1995**, *40*, 477−500.
(21) Lee, S. K.; Zu, Y.; Herrmann, A.; Geerts, Y.; Müllen, K.; Bard, A. J. Electrochemistry, Spectroscopy and Electrogenerated Chemiluminescence of Perylene, Terrylene, and Quaterrylene Diimides in Aprotic Solution. *J. Am. Chem. Soc.* **1999**, *121*, 3513−3520.
(22) Gregg, B. A.; Sprague, J.; Peterson, M. W. Long-Range Singlet Energy Transfer in Perylene Bis(phenethylimide) Films. *J. Phys. Chem. B* **1997**, *101*, 5362−5369.
(23) Ferrere, S.; Zaban, A.; Gregg, B. A. Dye Sensitization of Nanocrystalline Tin Oxide by Perylene Derivatives. *J. Phys. Chem. B* **1997**, *101*, 4490−4493.
(24) Rawls, M. T.; Johnson, J.; Gregg, B. A. Coupling One Electron Photoprocesses to Multielectron Catalysts: Towards a Photo-electrocatalytic System. *J. Electroanal. Chem.* **2010**, *650*, 10−15.
(25) Kanan, M. W.; Nocera, D. G. In Situ Formation of an Oxygen-Evolving Catalyst in Neutral Water Containing Phosphate and Co^{2+}. *Science* **2008**, *321*, 1072−1075.
(26) Du, P.; Kokhan, O.; Chapman, K. W.; Chupas, P. J.; Tiede, D. M. Elucidating the Domain Structure of the Cobalt Oxide Water Splitting Catalyst by X-Ray Pair Distribution Function Analysis. *J. Am. Chem. Soc.* **2012**, *134*, 11096−11099.
(27) Zhong, D. K.; Gamelin, D. R. Photoelectrochemical Water Oxidation by Cobalt Catalyst ("Co−Pi")/α-Fe_2O_3 Composite Photoanodes: Oxygen Evolution and Resolution of a Kinetic Bottleneck. *J. Am. Chem. Soc.* **2010**, *132*, 4202−4207.

(28) Marcon, R. O.; Brochsztain, S. Characterization of Self-Assembled Thin Films of Zirconium Phosphonate/Aromatic Diimides. *Thin Solid Films* **2005**, *492*, 30−34.
(29) Rodríguez-Abreu, C.; Aubery-Torres, C.; Solans, C.; López-Quintela, A.; Tiddy, G. J. T. Characterization of Perylene Diimide Dye Self-Assemblies and Their Use As Templates for the Synthesis of Hybrid and Supermicroporous Nanotubules. *ACS Appl. Mater. Interfaces* **2011**, *3*, 4133−4141.
(30) Shin, I.-S.; Hirsch, T.; Ehrl, B.; Jang, D.-H.; Wolfbeis, O. S.; Hong, J.-I. Efficient Fluorescence "Turn-On" Sensing of Dissolved Oxygen by Electrochemical Switching. *Anal. Chem.* **2012**, *84*, 9163−9168.
(31) Gregg, B. A.; Cormier, R. A. Liquid Crystal Perylene Diimide Films Characterized by Electrochemical, Spectroelectrochemical, and Conductivity versus Potential Measurements. *J. Phys. Chem. B* **1998**, *102*, 9952−9957.
(32) Bard, A. J.; Faulkner, L. R. *Electrochemical Methods: Fundamentals and Applications*, 2nd ed.; John Wiley & Sons: Hoboken, NJ, 2001.
(33) Gregg, B. A. Evolution of Photophysical and Photovoltaic Properties of Perylene Bis(phenethylimide) Films upon Solvent Vapor Annealing. *J. Phys. Chem.* **1996**, *100*, 852−859.
(34) Cormier, R. A.; Gregg, B. A. Self-Organization in Thin Films of Liquid Crystalline Perylene Diimides. *J. Phys. Chem. B* **1997**, *101*, 11004−11006.
(35) Cormier, R. A.; Gregg, B. A. Synthesis and Characterization of Liquid Crystalline Perylene Diimides. *Chem. Mater.* **1998**, *10*, 1309−1319.
(36) Gregg, B. A.; Kose, M. E. Reversible Switching between Molecular and Charge Transfer Phases in a Liquid Crystalline Organic Semiconductor. *Chem. Mater.* **2008**, *20*, 5235−5239.
(37) Kazmaier, P. M.; Hoffmann, R. A Theoretical Study of Crystallochromy. Quantum Interference Effects in the Spectra of Perylene Pigments. *J. Am. Chem. Soc.* **1994**, *116*, 9684−9691.
(38) Stenzel, O. Solid State Optics. In *The Physics of Thin Film Optical Spectra: An Introduction*; Ertl, G., Luth, H., Mills, D. L., Eds.; Springer Series in Surface Sciences; Springer-Verlag: Berlin, 2005; Vol. *44*, pp 199−288.
(39) Cardona, C. M.; Li, W.; Kaifer, A. E.; Stockdale, D.; Bazan, G. C. Electrochemical Considerations for Determining Absolute Frontier Orbital Energy Levels of Conjugated Polymers for Solar Cell Applications. *Adv. Mater.* **2011**, *23*, 2367−2371.
(40) Johansson, T.; Mammo, W.; Svensson, M.; Andersson, M. R.; Inganäs, O. Electrochemical Bandgaps of Substituted Polythiophenes. *J. Mater. Chem.* **2003**, *13*, 1316−1323.
(41) Zahn, D. R. T.; Gavrila, G. N.; Gorgoi, M. The Transport Gap of Organic Semiconductors Studied Using the Combination of Direct and Inverse Photoemission. *Chem. Phys.* **2006**, *325*, 99−112.
(42) Hains, A. W.; Liang, Z.; Woodhouse, M. A.; Gregg, B. A. Molecular Semiconductors in Organic Photovoltaic Cells. *Chem. Rev.* **2010**, *110*, 6689−6735.
(43) Park, Y.; Choong, V.; Gao, Y.; Hsieh, B. R.; Tang, C. W. Work Function of Indium Tin Oxide Transparent Conductor Measured by Photoelectron Spectroscopy. *Appl. Phys. Lett.* **1996**, *68*, 2699−2701.
(44) Steinmiller, E. M. P.; Choi, K.-S. Photochemical Deposition of Cobalt-Based Oxygen Evolving Catalyst on a Semiconductor Photoanode for Solar Oxygen Production. *Proc. Natl. Acad. Sci. U.S.A.* **2009**, *106*, 20633−20636.
(45) Salvador, P.; Gutiérrez, C. Analysis of the Transient Photocurrent-Time Behaviour of a Sintered n-$SrTiO_3$ Electrode in Water Photoelectrolysis. *J. Electroanal. Chem. Interfacial Electrochem.* **1984**, *160*, 117−130.
(46) Chen, Z.; Jaramillo, T. F.; Deutsch, T. G.; Kleiman-Shwarsctein, A.; Forman, A. J.; Gaillard, N.; Garland, R.; Takanabe, K.; Heske, C.; Sunkara, M.; McFarland, E.; Domen, K.; Miller, E.; Turner, J.; Dinh, H. Accelerating Materials Development for Photoelectrochemical Hydrogen Production: Standards for Methods, Definitions, and Reporting Protocols. *J. Mater. Res.* **2010**, *25*, 3−16.
(47) Demmig, S.; Langhals, H. Very Soluble and Photostable Perylene Fluorescent Dyes. *Chem. Ber.* **1988**, *121*, 225−230.
(48) Falck, D. Amperometric Oxygen Electrodes. *Curr. Sep.* **1997**, *16*, 19−22.
(49) U.S. Geological Survey. Dissolved Oxygen Solubility Tables http://water.usgs.gov/software/DOTABLES/ (accessed Jun 7, 2013).